Available online at www.sciencedirect.com
ScienceDirect
Journal of Power Sources 160 (2006) 1230–1241
JOURNAL OF POWER SOURCES
www.elsevier.com/locate/jpowsour

On the start-up transient simulation of a turbo fuel cell system

Po-Hsu Lin, Che-Wun Hong *

Department of Power Mechanical Engineering, National Tsing Hua University, 101, Sec. 2, Kwang Fu Road, Hsinchu 30013, Taiwan

Received 3 November 2005; received in revised form 9 February 2006; accepted 10 February 2006
Available online 31 March 2006

Abstract

The start-up transient behavior is an important issue in a turbo fuel cell system design. This paper developed a general dynamic model of the hybrid fuel cell/micro-gas turbine (MGT) system to investigate the transient behavior during cold start. The unsteady flow process through components of the turbo fuel cell system, which includes a solid oxide fuel cell (SOFC) stack, an afterburner, a turbo generator and heat exchangers, was modeled using a filling-and-emptying approach. Each major component was treated as a function block in the coded model. Computer simulations were performed on a Matlab/Simulink platform based on the block-diagram concept. The main focus of this study is on the start-up transient behavior of a basic turbo fuel cell system. The simulation results show that the start-up time for the example turbo fuel cell system (200 kW SOFC plus 50 kW MGT) can be up to about a few hours. Preliminary parametric investigations with different operating conditions show that the start-up duration can be reduced to less than 1 h.

Keywords: SOFC; MGT; Dynamic model; Filling-and-emptying approach

1. Introduction

Fuel cells are the most promising technology for the next generation of power plants with high efficiency and extremely low pollution. Due to the wide range of power outputs, fuel cells have many applications from small scale, such as telecommunications, to large scale, e.g., electric vehicles and distributed power stations. Among many types of fuel cells, solid oxide fuel cells (SOFCs) have the highest efficiency because of high temperature operation, typically between 600 °C and 1000 °C. The high operating temperature enables the exhaust energy from the SOFC to be recovered by other components, such as recuperators and turbochargers. A hybrid power generation system, combining the SOFC with a micro-gas turbine (MGT), called the turbo fuel cell system, has been proposed. It has been extensively studied in recent years because of its excellent system efficiency—of up to 80% [1]. However, the hybrid system suffers from the slow response due to thermal lag, turbo lag and some parasitic losses. Hence, cold start transient is an important issue in designing such a power generation system.

Computer simulations, under steady and transient condition, are normally the first step to design the performance and to determine the specification of the hybrid system. In some studies, linear dynamic models of the SOFC were constructed, using system identification algorithms to study the steady performance of the hybrid fuel cell system [2,3]. Aguiar et al. [4] and Recknagle et al. [5] built up a thermofluid electrochemical model for SOFC stacks based on the energy conservation law. They also aimed for studying the steady state performance to achieve the best efficiency. In 2003, Petruzzi et al. [6] developed an SOFC model to investigate the fuel cell performance under different operating conditions, including start-up, idling and cooling down. Chan et al. [7] studied the steady state performance of a hybrid fuel cell system with a simple SOFC model and a static performance map of the turbocharger. In 2004, Magistri et al. [8,9] derived a simplified SOFC dynamic model with anode recirculation to investigate the transient system dynamics. Bohn and Pöppe [10] studied the performance of an integration of an SOFC and a micro-turbine with and without heat exchangers. Nishida et al. [11] tried to redesign the turbo fuel cell system and showed that a multi-stage system had a better thermal efficiency than the single-stage one.

Although system matching and configuration designs were studied, the cold start-up transient of the turbo fuel cell system, an important topic, has not been thoroughly addressed. In this

* Corresponding author. Tel.: +886 3 5742591; fax: +886 3 5722840.
E-mail address: cwhong@pme.nthu.edu.tw (C.-W. Hong).

0378-7753/$ – see front matter © 2006 Elsevier B.V. All rights reserved.
doi:10.1016/j.jpowsour.2006.02.030

Nomenclature

A	exchange area of heat exchangers (m^2)
A, B, C, D, E	coefficients of the reforming and water–gas shifting reaction
c_p	specific heat ($kJ\,kg^{-1}\,K^{-1}$)
E	output voltage of solid oxide fuel cell (V)
E_{ideal}	ideal voltage of solid oxide fuel cell (V)
F	air–fuel ratio
Fa	Faraday constant ($C\,mol^{-1}$)
ΔG°	Gibbs free energy (J)
h	enthalpy ($kJ\,kg^{-1}$)
i_0	exchange current density ($A\,cm^{-2}$)
i_{limit}	limiting current density of fuel cell ($A\,cm^{-2}$)
i	current command (A)
K_p	chemical equilibrium constant
m	mass (kg)
n	number of transfer electrons
N^i	inlet mole flow rate ($mol\,s^{-1}$)
P	pressure (kPa)
$\dot{q}_{ec}$	heat released from the electrochemical reaction ($J\,s^{-1}$)
$\dot{q}_{re}$	heat absorbed by the reforming reaction ($J\,s^{-1}$)
$\dot{q}_{tr}$	heat transferred between the gas and the channel wall ($J\,s^{-1}$)
$\dot{q}_{ws}$	heat released from the water–gas shifting reaction ($J\,s^{-1}$)
Q	heat transfer (J)
R	gas constant ($J\,mol^{-1}\,K^{-1}$)
R_{ohm}	fuel cell electric resistance
t	elapsed time (s)
T	temperature (V)
ΔT_m	suitable mean temperature difference in the heat exchanger
u	internal energy (J)
U	heat exchange coefficient
V	volume (m^3)
W	power (W)
x, y, z	reaction rate of reforming reaction, water–gas shifting reaction and electrochemical reaction ($mol\,s^{-1}$)

Greek letters

α	charge transfer coefficient
γ	specific heat ratio
ε	heat exchanger effectiveness
η_{act}	activation overpotential (V)
η_c	isentropic efficiency of compressor
η_{con}	concentration overpotential (V)
η_{ohm}	ohmic overpotential (V)
η_T	isentropic efficiency of turbine

Subscripts

atm	atmosphere
C	compressor
c	cold
cell	solid oxide fuel cell
comb	combustor
ds	downstream
h	hot
i	inlet
j	species of inlet gas
m	mechanical
o	outlet
sf	heat transfer surface of the control volume
T	turbine

study, a non-linear system dynamic model was developed to simulate the dynamic performance of a 250 kW turbo fuel cell system (200 kW SOFC plus 50 kW MGT). It is based on a filling-and-emptying approach, which was developed for turbocharged engine system design before [12,13]. Although configuration matching and optimal performance design are also the functions of this dynamic package, the start-up transient is the topic what we focus on in this paper.

2. Hybrid system modeling

Fig. 1 shows the basic configuration of a turbo fuel cell system. The system consists of two heat exchangers, an SOFC stack, a combustor, a compressor and a turbo generator. The methane fuel and the compressed air pass through the heat exchanger to recover the heat energy from the high-temperature exhaust. The water vapor is generated through the other heat exchanger to join the internal reforming inside the SOFC stack. After the electrochemical reaction taking place, the remaining fuel and the excess air leave the SOFC stack and enter the combustor. The gas mixture combusts and releases the chemical energy that increases the enthalpy and temperature of the whole system. The high-temperature, high-enthalpy gas expands via the turbine which then drives the air compressor and the electric generator simultaneously. In this paper, a dynamic model of this turbo fuel cell system was constructed following the fuel, the air and the gas mixture loops as shown in Fig. 1.

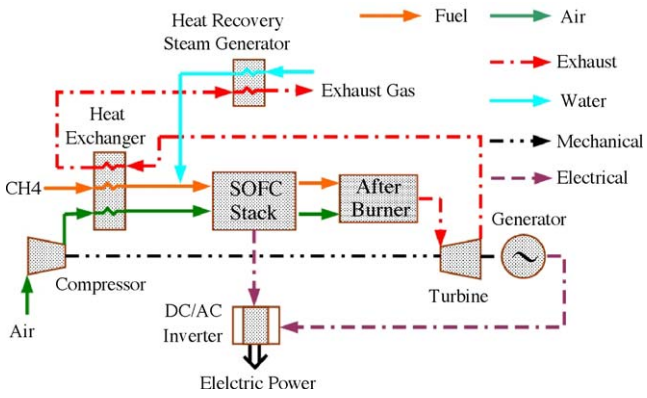

Fig. 1. Flow diagram of a typical turbo fuel cell system.

2.1. Filling and emptying model

To model the electrochemical thermodynamics cycle of the hybrid fuel cell system, a filling-and-emptying model [12,13] which was developed for turbocharged engines originally was adopted. The general model follows the mass continuity and energy conservation laws. It is expressed in the manner of dynamics (function of time) for the unsteady flow of an open system:

$$\frac{dm}{dt} = \sum_j \frac{dm_j}{dt} \tag{1}$$

$$\frac{dT}{dt} = \left[-\frac{RT}{V}\frac{dV}{dt} + \left(\sum_{sf} \frac{dQ_{sf}}{dt} + \sum_j h_{oj}\frac{dm_j}{dt} - u\frac{dm}{dt} \right)\frac{1}{m} - \frac{\partial u}{\partial F}\frac{dF}{dt} \right] \Big/ \frac{\partial u}{\partial T} \tag{2}$$

where $\sum_j dm_j/dt$ is the summation of the mass that enters and leaves the control volume. The term $(RT/V)(dV/dt)$ is neglected due to the constant system volume; $\sum_{sf} dQ_{sf}/dt$ is the heat transfer through the surfaces of the control volume; $\sum_j h_{oj}(dm_j/dt)$ the sum of the change of the specific stagnation enthalpy, due to the mass flow in and out of the volume; $u(dm/dt)$ the internal energy variation due to the mass change; and $(\partial u/\partial F)(dF/dt)$ is the change of the internal energy due to the air–fuel ratio variation. However, the volume in the turbo fuel cell system remains constant, so the term $(RT/V)(dV/dt)$ is negligible. The air–fuel ratio term $(\partial u/\partial F)(dF/dt)$ is also negligible because the equivalent ratio is almost fixed during the operation. Therefore, Eq. (2) can be simplified to be

$$\frac{dT}{dt} = \frac{\left(\sum_{sf} dQ_{sf}/dt + \sum_j dm_j/dt - u(dm/dt) \right)(1/m)}{\partial u/\partial T} \tag{3}$$

The pressure dynamics can then be derived from the state equation of the ideal gas, which takes the form of:

$$\frac{dP}{dt} = P\left(\frac{1}{m}\frac{dm}{dt} + \frac{1}{T}\frac{dT}{dt} \right) \tag{4}$$

Fig. 2 shows the block diagram of the simulation process based on the Matlab/Simulink platform. Each block represents a major component corresponding to the hardware in Fig. 1. The blocks can be moved around for configuration design and system matching. The following sections describe the thermal flow process and performance evaluation in each component.

2.2. Solid oxide fuel cell

For an SOFC system fed with the methane, a reforming process is required to produce the hydrogen fuel. In this study,

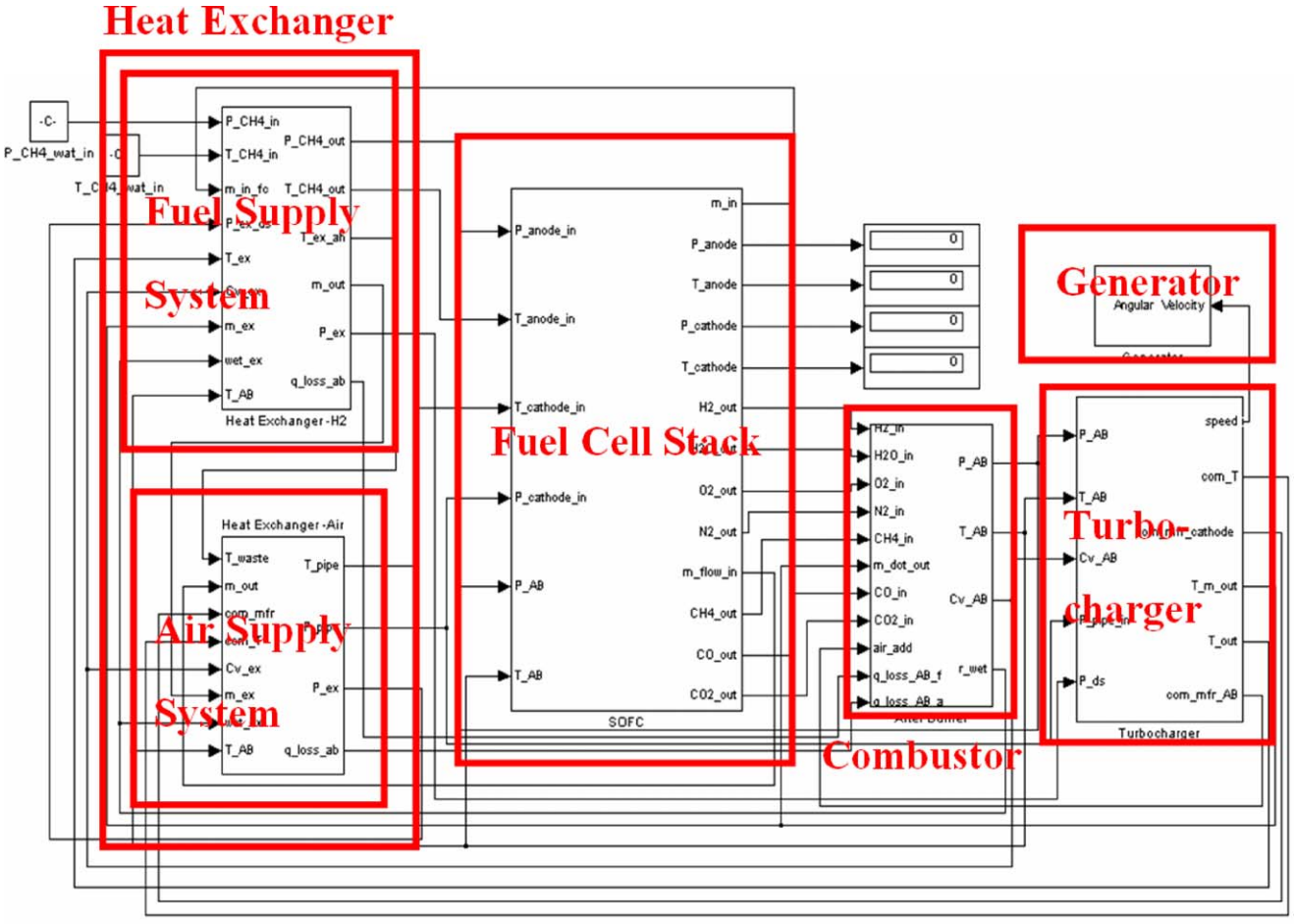

Fig. 2. Block diagram of the turbo fuel cell simulation on the Matlab/Simulink platform.

an internal reforming mechanism was identified due to high temperature operation. The reforming mechanism includes two chemical reactions; they are:

$$CH_4 + H_2O \rightarrow CO + 3H_2, \quad \text{reforming} \tag{5}$$

$$CO + H_2O \rightarrow CO_2 + H_2, \quad \text{water–gas shifting} \tag{6}$$

The equilibrium constants of the reactions can be derived by

$$K_{p,\text{reform}} = \frac{((N^{\text{i}}_{\text{CO}} + x - y)/(N^{\text{i}}_{\text{total}} + 2x))((N^{\text{i}}_{\text{H}_2} + 3x + y - z)/(N^{\text{i}}_{\text{total}} + 2x))^3}{((N^{\text{i}}_{\text{CH}_4} - x)/(N^{\text{i}}_{\text{total}} + 2x))((N^{\text{i}}_{\text{H}_2\text{O}} - x - y + z)/(N^{\text{i}}_{\text{total}} + 2x))} P^2_{\text{cell}},$$

$$K_{p,\text{shifting}} = \frac{((N^{\text{i}}_{\text{CO}_2} + y)/(N^{\text{i}}_{\text{total}} + 2x))((N^{\text{i}}_{\text{H}_2} + 3x + y - z)/(N^{\text{i}}_{\text{total}} + 2x))}{((N^{\text{i}}_{\text{CO}} + x - y)/(N^{\text{i}}_{\text{total}} + 2x))((N^{\text{i}}_{\text{H}_2\text{O}} - x - y + z)/(N^{\text{i}}_{\text{total}} + 2x))} \tag{7}$$

where N is the number of moles, and the subscripts CO, CH_4, CO_2, H_2 and H_2O indicate the gas components that participate in the reactions. The term $N^{\text{i}}_{\text{total}}$ represents the total mole flow rates of the inlet gas mixture including the methane and the steam vapor. The variables x, y and z are the reaction rates of the reforming reaction, the water–gas shifting reaction and the electrochemical reaction, respectively. Also, the equilibrium constants can be expressed as a function of temperature

$$\log K_p = AT^4 + BT^3 + CT^2 + DT + E \tag{8}$$

Table 1 provides the constants A–E [14] in Eq. (8) for these two chemical reactions. The reaction rate z is determined from the current command i:

$$z = \frac{i}{n\text{Fa}} \tag{9}$$

where n is the number of transfer electrons and Fa is the Faraday constant. The reaction rates, x and y, can be determined from Eq. (7). Hence, the change of number of moles of each gas component in the anode can be obtained by

$$\begin{aligned} N_{\text{CH}_4} &= N^{\text{i}}_{\text{CH}_4} - x, \qquad N_{\text{CO}} = N^{\text{i}}_{\text{CO}} + x - y, \\ N_{\text{CO}_2} &= N^{\text{o}}_{\text{CO}_2} + y, \qquad N_{\text{H}_2} = N^{\text{o}}_{\text{H}_2} + 3x + y - z, \\ N_{\text{H}_2\text{O}} &= N^{\text{o}}_{\text{H}_2\text{O}} - x - y + z \end{aligned} \tag{10}$$

where the superscripts 'i' and 'o' represent the inlet and outlet, respectively.

The temperature and pressure variation are calculated by Eqs. (3) and (4), but some additional mass and energy sources have to be included. Two heat source terms for reforming and water shifting reaction ($\dot{q}_{\text{re}}$ and $\dot{q}_{\text{ws}}$) are added to Eq. (3), because the internal reforming reaction is endothermic. An additional heat source term is the exothermic electrochemical reaction, $\dot{q}_{\text{ec}}$. The electrochemical reaction is

$$\begin{aligned} &\text{Anode} &&: 2H_2 + 2O^{2-} \rightarrow 2H_2O + 4e^- \\ &\text{Cathode} &&: N_2 + O_2 + 4e^- \rightarrow 2O^{2-} + N_2 \\ &\text{Overall} &&: 2H_2 + O_2 + N_2 \rightarrow 2H_2O + N_2 \end{aligned} \tag{11}$$

The heat transfer ($\dot{q}_{\text{tr}}$) between the gases and the channel wall must also be considered. Oxygen ions are transferred from the cathode to the anode, so the energy transfer associated with the oxygen transfer also has to be considered.

The ideal voltage of the SOFC is determined from the Nernst equation

$$E_{\text{ideal}} = \frac{-\Delta G^\circ}{2\text{Fa}} + \frac{RT}{2\text{Fa}} \ln \frac{P_{\text{H}_2} P^{0.5}_{\text{O}_2}}{P_{\text{H}_2\text{O}}} - \frac{RT}{4\text{Fa}} \ln(P_{\text{cathode}}) \tag{12}$$

where the term $-\Delta G^\circ$ is the Gibbs free energy change which is varied with the operating temperature of the SOFC. The actual output voltage of the SOFC is evaluated by the ideal voltage minus those potential losses

$$E = E_{\text{ideal}} - \eta_{\text{act}} - \eta_{\text{con}} - \eta_{\text{ohm}} \tag{13}$$

where the term η_{act} is the activation overpotential, η_{con} the concentration overpotential and η_{ohm} is the ohmic overpotential. The overpotentials are given by

$$\eta_{\text{act}} = a + b \ln i, \quad \text{where } a \approx -\frac{RT}{n\alpha\text{Fa}} \ln i_{\text{o}} \text{ and } b \approx \frac{RT}{n\alpha\text{Fa}}$$

$$\eta_{\text{con}} = -\frac{RT}{n\text{Fa}} \ln\left(1 - \frac{i}{i_{\text{limit}}}\right)$$

$$\eta_{\text{ohm}} = i \cdot R_{\text{ohm}}$$

where α is the transfer coefficient, i_0 the exchange current density, i_{limit} the limiting current density and R_{ohm} is the total cell resistance, which depends on the fuel cell stack temperature. The current i is from the demanded load, which is set to be a function of time in our simulation.

Table 1
Coefficients of the equilibrium constants of the reforming and shifting process

	Reforming	Shifting
A	-2.63121×10^{-11}	5.47301×10^{-12}
B	1.24065×10^{-7}	-2.57479×10^{-8}
C	-2.25232×10^{-4}	4.63742×10^{-5}
D	-1.95028×10^{1}	-3.91500×10^{-2}
E	-6.61395×10^{1}	1.32097×10^{1}

2.3. Combustor (or after burner)

The unreacted fuel with the reaction products in the SOFC anode, including CH_4, CO and H_2, are fed into an after burner in which the combustible gases mixed with the excess air from the SOFC cathode are burned to utilize the residual chemical energy. The combustion reaction in the combustor includes

$$CH_4 + 2O_2 \rightarrow CO_2 + 2H_2O + q_{\text{comb,CH}_4} \tag{14}$$

$$2CO + O_2 \rightarrow 2CO_2 + q_{comb,CO} \quad (15)$$

$$2H_2 + O_2 \rightarrow 2H_2O + q_{comb,H} \quad (16)$$

where q_{comb,CH_4}, $q_{comb,CO}$ and q_{comb,H_2} are the apparent heat release of the fuels CH_4, CO and H_2, respectively. Complete combustion is assumed. The heat release terms in Eqs. (14)–(16) should be added to Eq. (3) to determine the temperature dynamics. The pressure dynamics is calculated by Eq. (4), which follows the ideal gas state equation.

2.4. Turbocharger and electric generator

The turbocharger system consists of an air compressor and a micro-gas turbine. The compressor is driven by the gas turbine via a mechanical shaft. The power required to drive the compressor at a specific pressure ratio can be expressed by

$$\dot{W}_C = c_{p_c} \cdot \dot{m}_C \cdot \frac{T_{atm}}{\eta_C} \left(\left(\frac{P_{C,ds}}{P_{atm}} \right)^{(\gamma-1)/\gamma} - 1 \right) \quad (17)$$

where subscript 'C' stands for the compressor, c_{p_c} the specific heat of the compressed air at constant pressure, γ the specific heat ratio, $\dot{m}_C$ the mass flow rate, η_C the compressor efficiency from the compressor map, $P_{C,ds}$ the downstream pressure of the compressor and T_{atm} and P_{atm} are the atmospheric temperature and pressure. The power generated at the gas turbine is recovered from the combustion product. It is calculated by the enthalpy drop across the turbine and takes the form:

$$\dot{W}_T = c_{pT} \cdot \dot{m}_T \cdot T_{comb} \cdot \eta_T \left(\left(\frac{P_{T,ds}}{P_{comb}} \right)^{(\gamma-1)/\gamma} - 1 \right) \quad (18)$$

where P_{comb} and T_{comb} represent the pressure and the temperature of the combustion product at the turbine inlet, $\dot{m}_T$ the mass flow rate, η_T the turbine efficiency, $P_{T,ds}$ the downstream pressure of the gas turbine (normally atmosphere) and c_{pT} is the specific heat of the turbine gas at constant pressure. In this research, compressor and turbine performance maps were scaled from an existing much smaller turbocharger. The mass flow rate, isentropic efficiency, η_C and η_T, were interpolated from the related database. The actual power delivered to the electric generator is the micro-turbine power subtracted by the compressor power, which is

$$\dot{W} = \eta_m(\dot{W}_T - \dot{W}_C) \quad (19)$$

where η_m is the mechanical efficiency, assumed to be 0.95. The mechanical power is then transferred to the electric power by an alternator. The inertia of the turbocharger and the generator are considered; hence, the rotational speed dynamics of the turbo generator system is influenced by the summation of the mechanical load and the electromagnetic load.

2.5. Heat exchanger

The heat exchanger equipped in the turbo fuel cell system is to recover part of the thermal energy from the high temperature turbine exhaust. It can be used to preheat the fuel and air flow before entering the high temperature fuel cell. Part of the purpose is to reduce the thermal lag of the inlet gas flow and to improve the transient response. The recovered heat power can be determined from the equivalent Newton's heat transfer equation

$$\dot{q}_{exchange} = \varepsilon \cdot U \cdot A \cdot \Delta T_m \quad (20)$$

where U is the overall heat transfer coefficient, A the surface area for heat transfer and ΔT_m is the suitable mean temperature difference across the heat exchanger. It is normally determined by the log mean temperature difference (LMTD), which is

$$\Delta T_m = \frac{\Delta T_2 - \Delta T_1}{\ln(\Delta T_2/\Delta T_1)}, \quad \Delta T_1 = T_{h,i} - T_{c,o},$$
$$\Delta T_2 = T_{h,o} - T_{c,i} \quad (21)$$

Subscripts 'h', 'c', 'i' and 'o' denote hot, cold, inlet and outlet, respectively. The heat exchanger effectiveness ε is defined as the actual heat transfer divided by the maximum possible heat transfer. It is normally a function of the exchanger design. A simple relation is $\varepsilon = 1 - \exp(-NTU)$, where NTU is the number of transfer units.

3. Simulation results

The above mathematical models were coded on a Matlab/Simulink platform. The numerical scheme ODE4 (Runge–Kutta) was employed. The static performance of a single-cell SOFC was predicted first to evaluate the temperature effect on the voltage–current relation. Fig. 3 shows that the higher the operation temperature, the lower the potential loss. Temperature higher than 1300 K may result in a sealing leakage problem, so the following transient simulations were carried out with the constraint of 1300 K maximum temperature. Table 2 shows the specification and operating conditions of a virtual turbo fuel cell system. The fuel cell is a co-flow 400-cell planar SOFC. The micro-turbine is scaled from an automotive

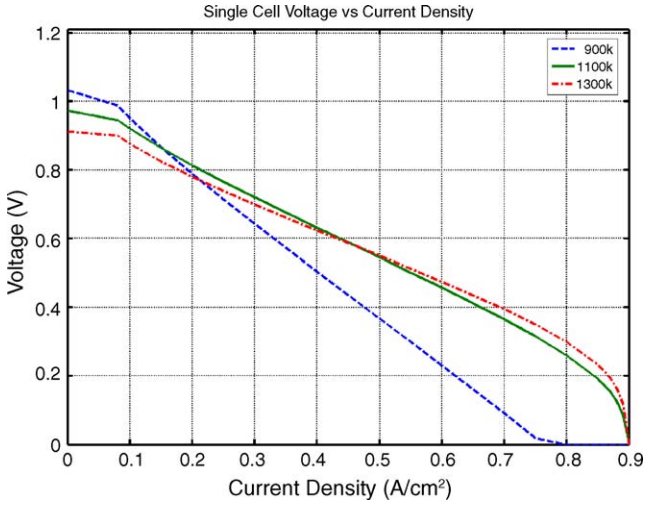

Fig. 3. Single cell voltage vs. current density at different temperatures showing the static performance of the SOFC.

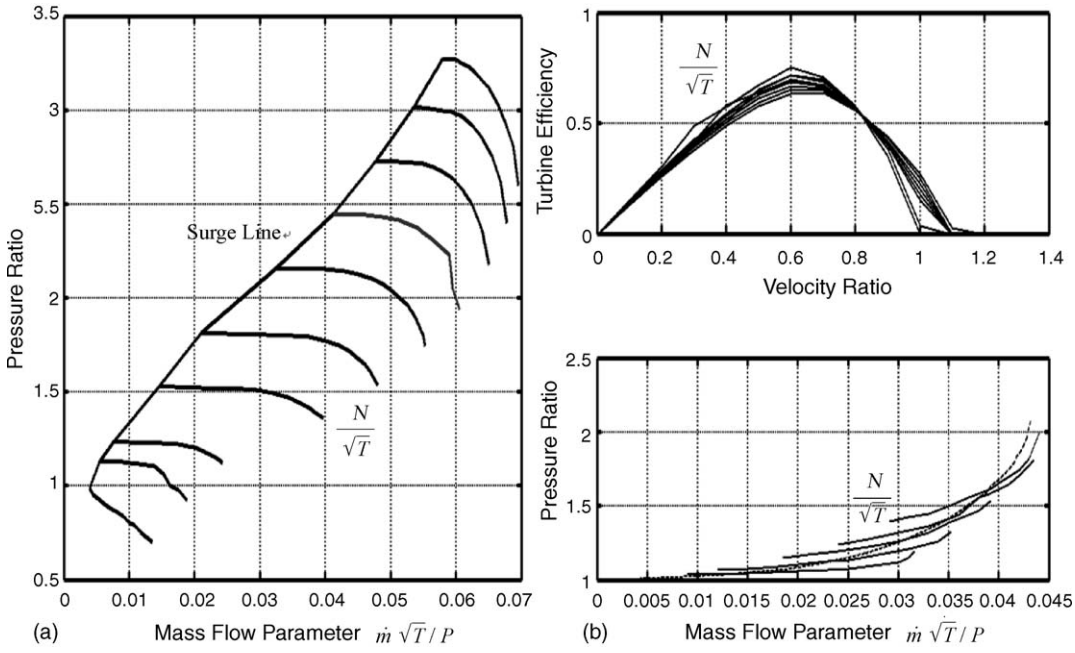

Fig. 4. Scaled turbocharger maps: (a) scaled mass flow parameter of compressor and (b) turbine maps.

diesel engine turbocharger. The scaled non-dimensional maps of the compressor and the turbine are shown in Fig. 4. The specification of the heat exchanger and the generator systems are from commercial products in the market.

Table 2
The specification and operating conditions of the turbo fuel cell system

Component	Specification and operating conditions
Solid oxide fuel cell	Type: co-flow planar SOFC The stack volume: 60 cm × 60 cm × 172 cm Single cell reaction area: 1900 cm^2 Numbers of cells: 400 Operation temperature: about 1250 K Fuel: methane or hydrogen Input pressure: 2–3 atm Input temperature: 300 K Oxidizer: air Initial pressure: 1 atm Initial temperature: 300 K Operation current density: 0.45 A cm^{-2} Maximum power: 260 kW
Combustor	Cylinder volume: 27,000 cm^3 Fuel: methane or hydrogen Oxidizer: air Initial composition: nitrogen 80%, oxygen 20%
Turbocharger	Radial type Rotational inertia, J: 1.63×10^{-3} kg m^2 Impeder and blade diameter: 7.0 cm
Heat exchanger	Inlet/outlet diameter: 15 cm Tube diameter: 5 cm
Electric generator	Limiting current: 300 A Resistance, R: 1.25 Ω Inductance, L_s: 0.012 H Torque constant, K_e: 1.25 V s rad^{-1} Rotational inertia, J: 2.1×10^{-1} kg m^2

3.1. Start-up transient simulation

The first topic to discuss is the transient response during the start-up period. This is a fundamental problem for high temperature fuel cells. In this hybrid system, we implement two heat exchangers and one combustor aiming to shorten the warm-up process. Fig. 5(a) shows that the SOFC starts to output voltage at the 1.3th hour, after warming up from ambient. This is because the electrochemical reaction has overcome the overpotential and reacts promptly when the stack temperature reaches 750 K. After that, the cell voltage increases with the stack temperature, and approaches constant at approximately 0.63 V for

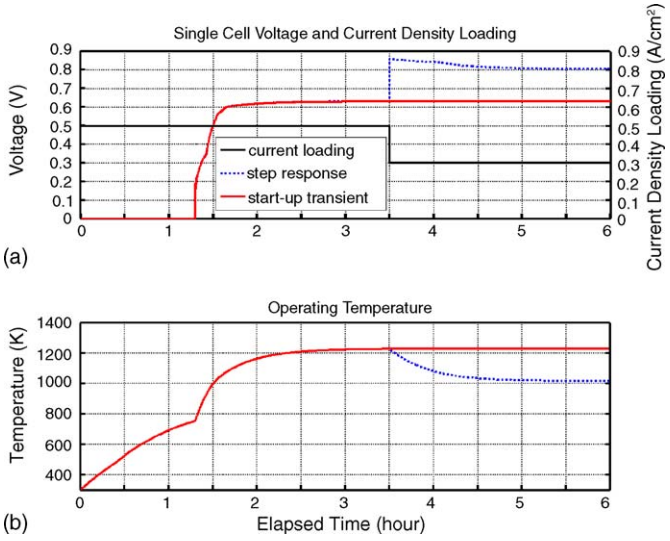

Fig. 5. Transient performance during start-up and step loading conditions: (a) single cell voltage and current density loading vs. elapsed time and (b) operating temperature vs. elapsed time.

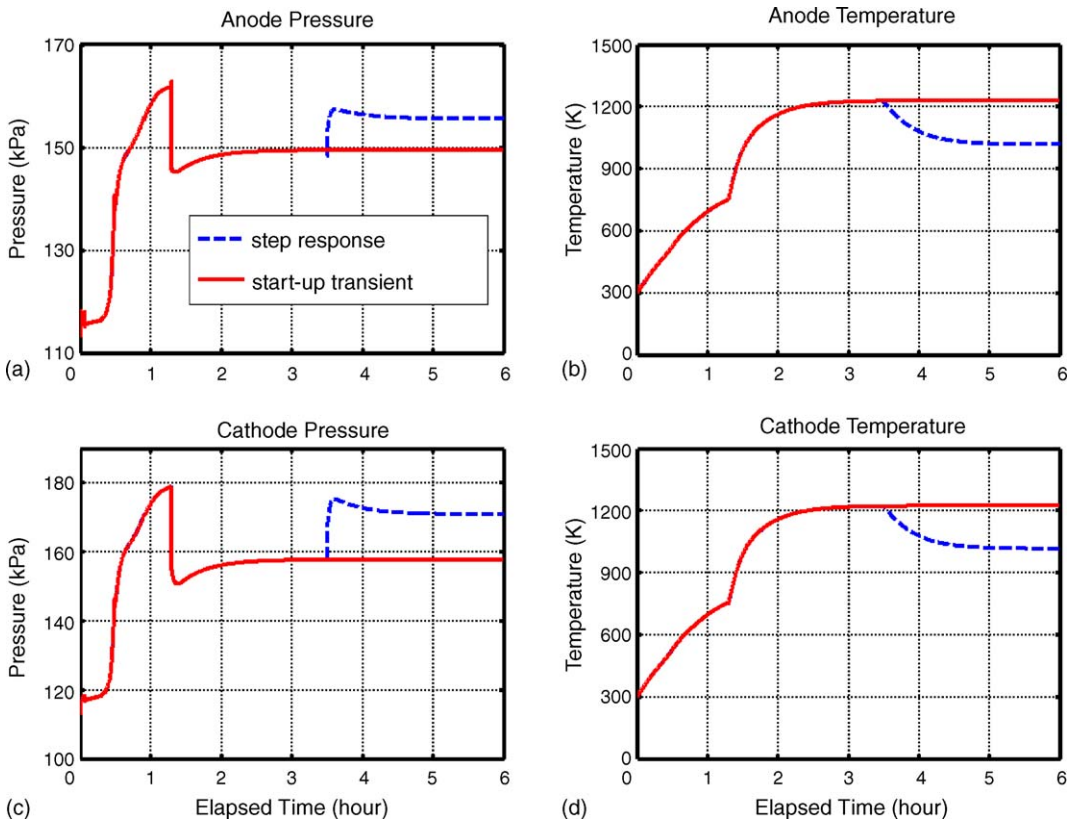

Fig. 6. (a) Anode pressure, (b) anode temperature, (c) cathode pressure and (d) cathode temperature dynamics during start-up and step loading conditions.

each cell. In Fig. 5(b), the stack temperature is raised from the ambient 300 K to 750 K during the first 1.3 h due to the recovered heat from the combustion exhaust. The slope of the stack temperature versus the elapsed time changes at the 1.3th hour. This is because the additional heat generated by the current with the overpotentials ($i\sum\eta$) is transferred to the SOFC stack. The stack temperature finally rises to about 1220 K and maintains constant due to thermal balance between the electrochemical heat release and the convection heat loss to the surroundings.

Fig. 6 illustrates the pressure and temperature dynamics at the anode and the cathode of the SOFC. The anode pressure and the cathode pressure, as shown in Fig. 6(a and c), continue to increase in the beginning because of the pressurized methane and the compressed air inlets. After the SOFC starts to react at the 1.3th hour, the pressure in both the anode and the cathode clearly decreases, because of the consumption of hydrogen and oxygen reactants. The water vapor is produced at the anode side, so the pressure drop in the cathode slightly exceeds that in the anode. In Fig. 6(b and d), the anode temperature and the cathode temperature change similarly with the stack temperature shown in Fig. 5(b). The temperature climbs over the first 1.3 h because the inlet fuel and air are preheated in the heat exchanger. The waste heat generated by the overpotentials after the first 1.3 h raises both the anode temperature and the cathode temperature.

Fig. 7(a) shows the pressurized methane inlet is preset at 2 atm. Fig. 7(b–d) shows the dynamics of the partial pressure of the composition such as the hydrogen, the water vapor and the methane in the anode. The hydrogen starts to produce when the internal reforming takes place as the stack temperature approaches 500 K. Fig. 7(b) shows that the hydrogen pressure decreases suddenly when the electrochemical reaction begins to react. Then, the hydrogen pressure increases and remains at constant when the internal reforming and the electrochemical reaction are balanced. In Fig. 7(c), the water vapor pressure increases initially because the vapor enters the anode with the methane. When the internal reforming reaction begins, the vapor pressure drops because the vapor is consumed in the reaction. When the fuel cell starts working, the vapor pressure gradually rises because the electrochemical reaction produces the water vapor. The vapor pressure then remains constant after 1.4 h. In Fig. 7(d), the methane pressure increases in the beginning because the pressurized methane flows into the anode. As the stack temperature approaches 500 K, the methane pressure decreases gradually because of internal reforming. The maximum consumption rate of the methane in the internal reforming reaction exceeds the inlet flow rate, so the methane pressure drops to zero.

Fig. 8(a) shows that the cathode pressure increases gradually because the compressor pressurizes the air. In Fig. 8(b), the oxygen consumption rate exceeds the inlet flow rate, so the oxygen pressure decreases when the electrochemical reaction starts. The drop in air pressure is partially responsible for the oxygen pressure drop, as shown in Fig. 8(a). Nitrogen does not participate in any chemical reaction, so its pressure simply varies with the air pressure in Fig. 8(c). Fig. 8(d) shows the dissipation power generated by the overpotential which is wasted through the heat

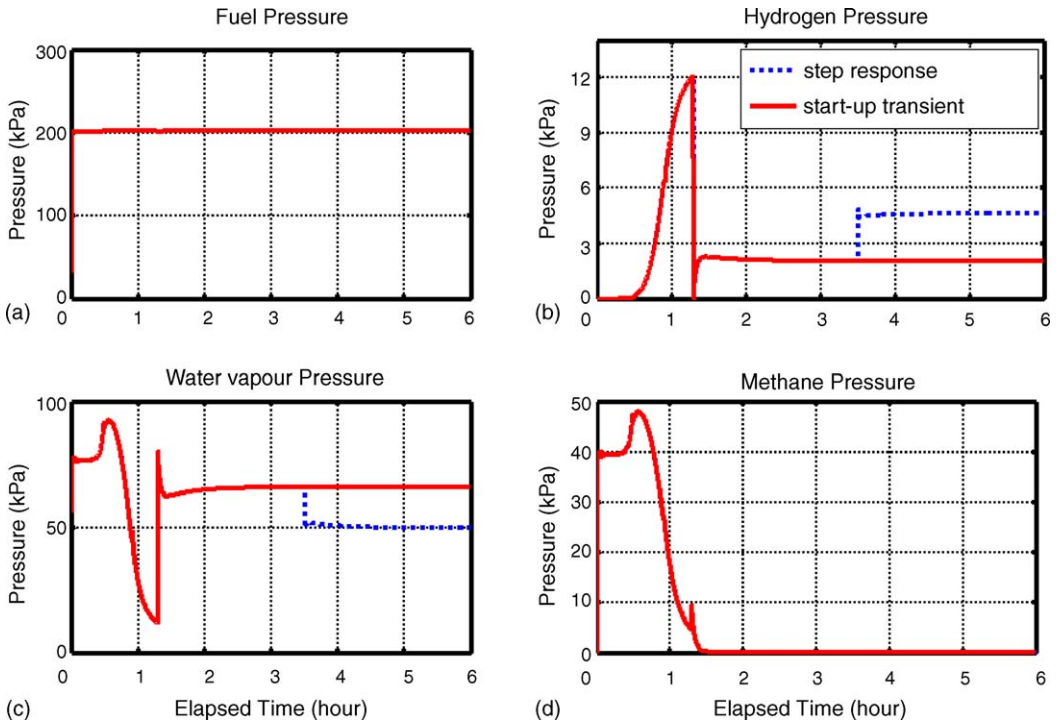

Fig. 7. Dynamics of the total pressure of (a) the fuel, and the partial pressure of (b) the hydrogen, (c) the water vapor and (d) the methane at the anode.

transfer process. As the SOFC voltage increases gradually, the overpotential drops to a small value. Therefore, the dissipation heat power decreases with time, as plotted in Fig. 8(d).

Fig. 9(a) plots the pressure dynamics inside the combustor. In Fig. 9(b), the combustor temperature indicates the mass averaged temperature between the reactants and the combustion products. The inlet mass flow rate exceeds the mass flow rate out of the combustor, so the pressure gradually rises. The temperature increases because of the chemical energy released from the combustion process. The temperature then decreases after the SOFC starts because the amount of unused fuels that flows into the combustor decreases. In Fig. 9(c), the angular velocity

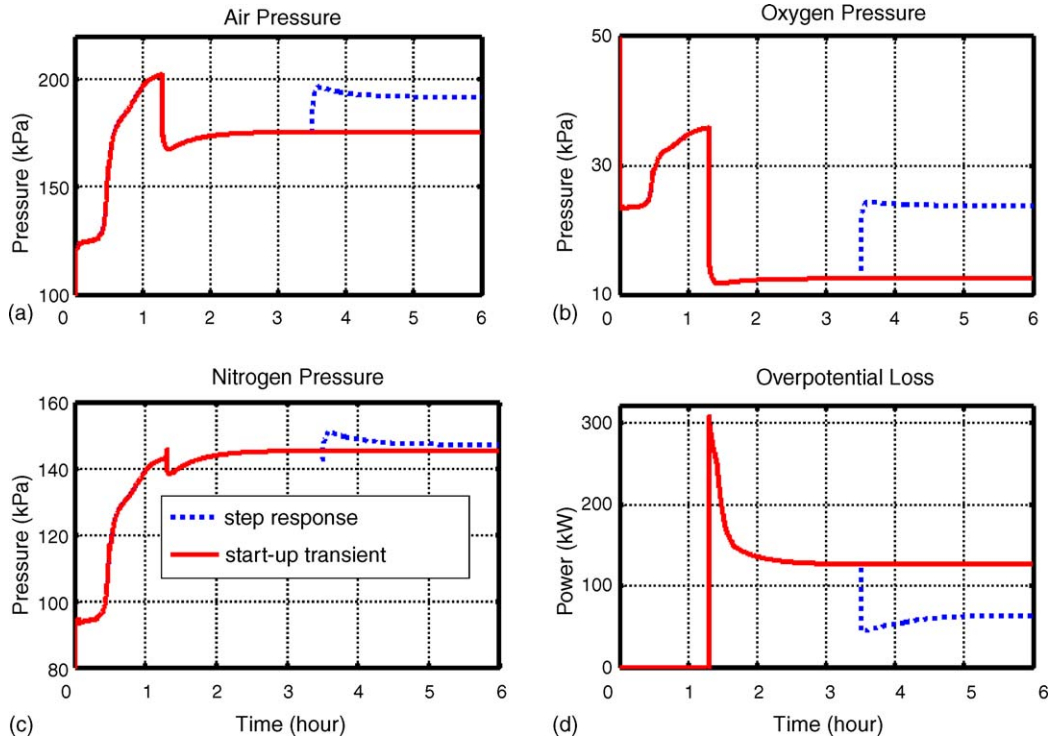

Fig. 8. Dynamics of (a) the air pressure, and partial pressure of (b) the oxygen, (c) the nitrogen inside the cathode and (d) the power loss due to the overpotentials.

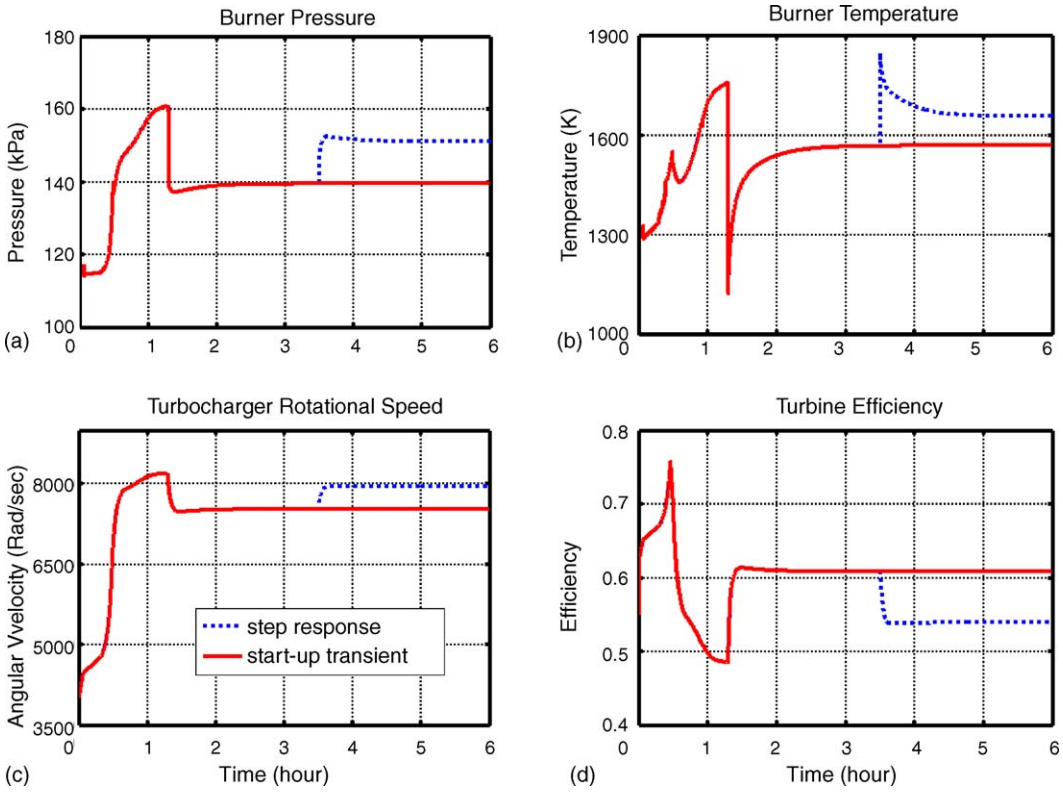

Fig. 9. (a) Pressure and (b) temperature dynamics of the combustor; (c) rotational speed and (d) efficiency of the micro-turbine.

of the turbocharger is initially 3500 rad s^{-1} (or 33,000 rpm), and then increases to almost 8200 rad s^{-1} (or 78,000 rpm) and stabilized at 7500 rad s^{-1} (or 72,000 rpm). The recovered power is basically proportional to the inlet temperature of the turbine, according to Eq. (18). In the simulation, the combustor temperature increases with time, so the recovered power also increases. The increased power accelerates the turbine, as shown in Fig. 9(c). Fig. 9(d) shows the variation of the turbine efficiency. The efficiency is simply determined from the performance map with the input of the rotational speed, the combustor temperature, the pressure ratio and the mass flow parameter.

3.2. Transient simulation with step load change

Step response is also one of the important transient performances. In this paper, the dynamic performance of the turbo fuel cell system is simulated with a varying current load with respect to the elapsed time. The current load decreases from 0.5 A cm^{-2} to 0.3 A cm^{-2} stepwise at the 3.5th hour. The dashed lines from Figs. 5–9 plot the transient response of the hybrid system. In Fig. 5, the voltage rises from 0.63 V to 0.85 V at the 3.5th hour and then slightly decreases to a constant value. Fig. 5 also shows the variation of the stack temperature caused mainly by the variation of the overpotentials. The drop of the overpotentials increases the cell voltage. Therefore, the waste heat added to the SOFC stack becomes lower when the current load decreases. Fig. 5 shows that the stack temperature decreases as less waste heat is generated, as the current load decreases.

The consumption rate of the reactants is proportional to the current load. The consumption of hydrogen and oxygen decreases as the current load becomes smaller. Therefore, the pressure of the anode and the cathode increases according to Eq. (4). The dashed line in Fig. 6(a and c) shows the anode and cathode pressure dynamics during the step load change. A lower current density also means that the electrochemical reaction releases less heat, so the temperature inside the anode and cathode is lower, as shown in Fig. 6(b and d).

The methane pressure remains constant as the current load is varied, as shown in Fig. 7(a). As discussed in the preceding paragraph, the rate of consumption of hydrogen is directly proportional to the current load. Less hydrogen is consumed when the current load is lower, so the pressure increases to a higher value. The rate of generation of water vapor is also directly proportional to the current load, so the variation of the vapor pressure follows the current load, as shown in Fig. 7(c) by the dashed line. The inlet methane reacts completely in the internal reforming reaction after 1.3 h, so the methane does not respond to the variation of the current density, as shown in Fig. 7(d).

The cathode pressure variation plotted in Fig. 8(a) depends on the rotational speed of the turbocharger, as shown in Fig. 9(c). Increasing the rotational speed causes the compressor to pressurize the air to a higher pressure, increasing the pressure in the cathode. Oxygen is the other reactant in the electrochemical reaction, so reducing the current load reduces the consumption of oxygen as well. The nitrogen does not participate in any reaction, so the variation in pressure simply changes with the cathode pressure. In Fig. 8(d), the waste heat generated by the overpoten-

tials varies with the current density. The overpotentials are also functions of the stack temperature, so the waste heat exhibits a transient variation versus the current load variation (Fig. 8(d)).

Fig. 9(a and b) illustrates the pressure and temperature dynamics inside the combustor. When the current load falls, increasing both the anode and cathode pressures also increases the mass flow rate into the combustor, so the combustor pressure increases. Fig. 9(b) shows the variation of the combustor temperature. The flow rates of unused hydrogen and oxygen into the combustor increase as the current load decreases, suggesting that more heat is released and the combustor temperature increases. In contrast, the temperature decreases as the current load increases. Fig. 9(b) shows a transient variation that occurs after the current density changes. Because the energy inside the combustor gradually converges to a constant value, so the temperature also converges to a constant value. In Fig. 9(c), the rotational speed of the turbocharger increases from 7300 rad s^{-1} to 8000 rad s^{-1} at the 3.5th hour. The efficiency in Fig. 9(d) falls to 0.54 at the 3.5th hour.

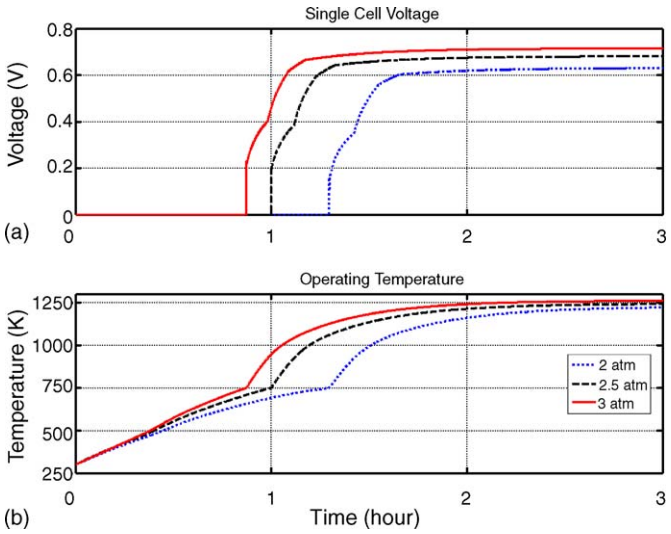

Fig. 10. Start-up transient simulation of (a) cell voltage and (b) stack temperature of the turbo SOFC under different fuel inlet pressure conditions.

3.3. Start-up simulation with higher fuel inlet pressure

The baseline start-up simulation presets the fuel inlet pressure to be at 2 atm. It is shown that the transient performance is sensitive to the fuel inlet pressure in the previous section. The inlet pressure of the methane is easy to control in the real operation. Hence, this section studies start-up behavior with two more fuel inlet pressures: 2.5 atm and 3 atm, respectively. Fig. 10 shows the predicted voltage and stack temperature dynamics. The SOFC has a shorter start-up time at a higher inlet fuel pressure, which also corresponds to a higher output voltage. The stack temperature curve in Fig. 10(b) shows that increasing the inlet fuel pressure also increases the slope of the temperature rise. As the slope increases, less time is needed to reach the temperature at which the electrochemical reaction can proceed.

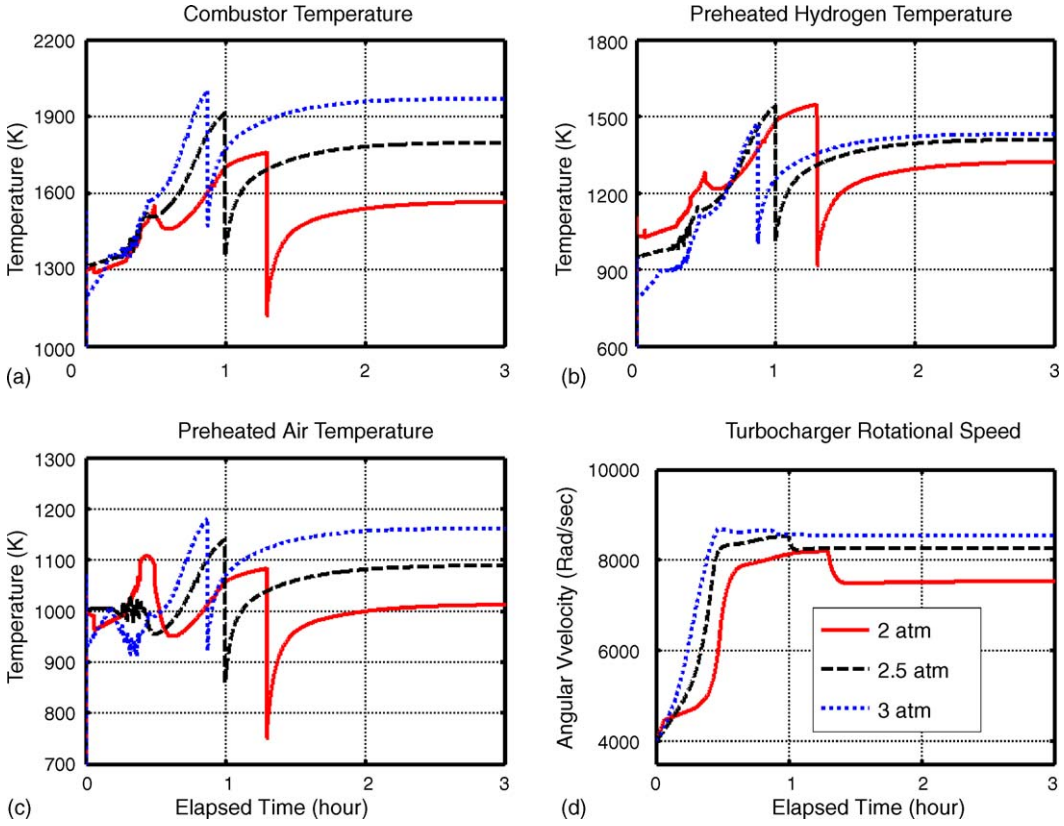

Fig. 11. Start-up transient simulation of (a) combustor temperature, (b) preheated hydrogen temperature, (c) preheated air temperature and (d) the turbine rotational speed under different fuel inlet pressure conditions.

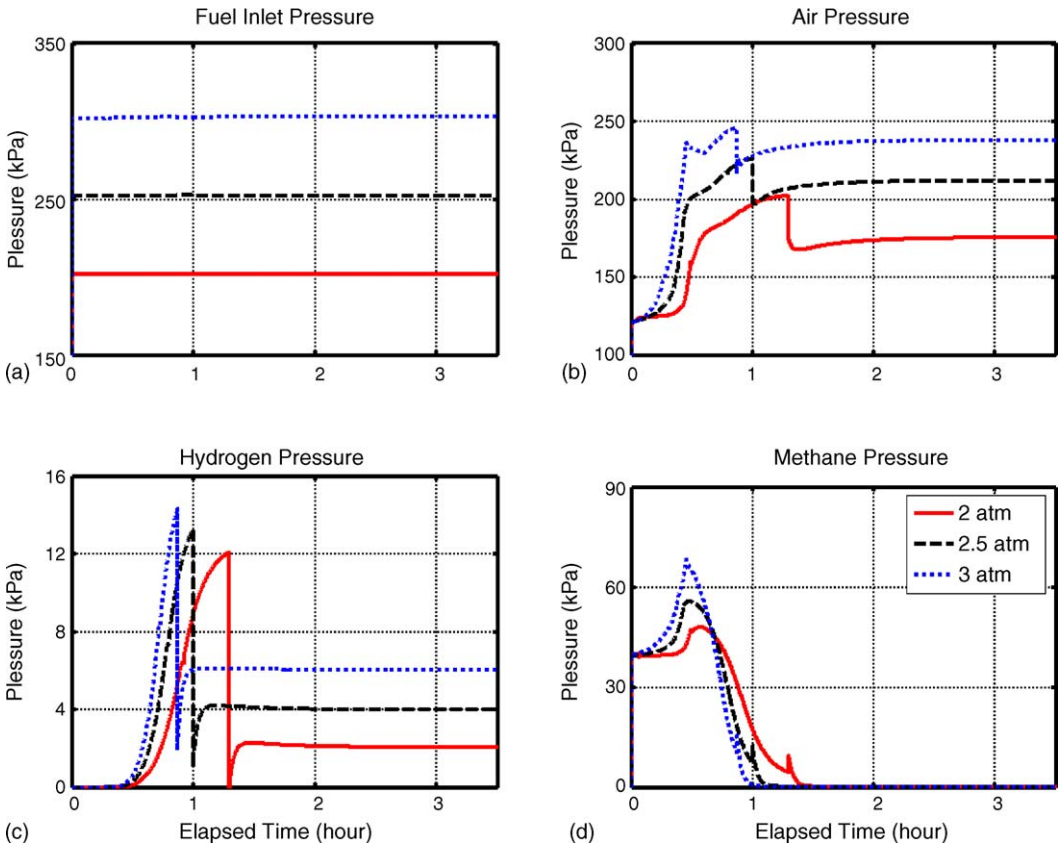

Fig. 12. Start-up transient simulation of (a) fuel inlet pressure, (b) compressed air, (c) the hydrogen in anode and (d) the methane in anode under different fuel inlet pressure conditions.

A higher fuel inlet pressure corresponds to the flowing of more unused fuel into the combustor. The extra fuel releases more heat, so the temperature inside the combustor is increased. The combustor temperature suddenly falls because the amount of unused fuel decreases after the SOFC starts up as shown in Fig. 11(a). Fig. 11(b and c) shows the temperature of the fuel and air downstream of the heat exchanger pipe. The fuel and air are heated to a higher temperature because of the exhaust gas from the turbine is hotter. The high temperature of the fuel and gas heats up the SOFC stack and reduces the start-up time. Fig. 11(d) plots the rotational speed of the turbocharger. The power recovered by the turbine is proportional to the input temperature, according to Eq. (18). When the combustor temperature increases with the inlet fuel pressure, more power is recovered, so the rotational speed increases.

Fig. 12 presents the transient simulation results at different locations with different fuel inlet pressures. The given fuel inlet pressures are 2 atm, 2.5 atm and 3 atm, as shown in Fig. 12(a). The higher turbo speed compresses the air to a higher value, so the air pressure of the cathode becomes higher, as shown in Fig. 12(b). Fig. 12(c) shows that the hydrogen pressure is proportional to the fuel inlet pressure. At a higher fuel inlet pressure, more methane flows into the anode, so the hydrogen pressure increases with the inlet fuel pressure. The methane is consumed at the anode and the amount available decreases to zero more quickly as the fuel inlet pressure is higher, as shown in Fig. 12(d).

4. Conclusions

A filling-and-emptying approach has been successfully employed to the dynamic simulation of an example 250 kW turbo fuel cell system. The mathematical model was coded and simulated on the Matlab/Simulink platform based on the block-diagram (control volumes and boundaries) concept. The conclusions drawn under various simulation conditions are as follows:

A. The start-up time of the 250 kW turbo fuel cell system (fuel inlet pressure was set to be 2 atm) is about 1.3 h. The generated power of the SOFC is approximately 200 kW and the micro-turbine is about 50 kW. The most important factor that affects the start-up time is the response of the stack temperature of the SOFC. The response lag can be reduced by the after burner design and the preheating of reactants, through the heat exchangers.
B. The transient response due to the step loading indicates that although the SOFC responds very quickly to the change in load, the temperature of each component in the system takes a long time to reach stabilization.
C. The start-up lag can be improved by increasing the fuel inlet pressure. When the fuel inlet pressure increases to 3 atm, the start-up duration of the turbo fuel cell system can be reduced to less than 1 h. This is an easy and effective way in practice to improve the slow start-up problem of the

turbo SOFC system. However, thermal concentration problems to sealing and effective heat transfer technique have to be solved beforehand. Further control strategy study is on-going to reduce the starting time to less than half an hour.

Acknowledgments

The authors would like to thank the National Science Council and the Institute of Nuclear Energy Research, Taiwan, for financially supporting this research under contracts of NSC93-2623-7-007-009-NU and NL940243 (94A00561J).

References

[1] DOE, Fuel Cell Handbook, seventh ed., November 2004.
[2] Y. Zhu, K. Tomsovic, Electr. Power Syst. Res. 62 (2002) 1–11.
[3] F. Jurado, J. Power Sources 129 (2004) 205–215.
[4] P. Aguiar, D. Chadwick, L. Kershenbaum, Chem. Eng. Sci. 57 (2002) 1665–1677.
[5] K.P. Recknagle, R.E. Williford, L.A. Chick, D.R. Rector, M.A. Khaleel, J. Power Sources 113 (2003) 109–114.
[6] L. Petruzzi, S. Cocchi, F. Fineschi, J. Power Sources 118 (2003) 96–107.
[7] S.H. Chan, H.K. Ho, Y. Tian, Int. J. Hydrogen Energy 28 (2003) 889–900.
[8] L. Magistri, F. Trasino, P. Costamagna, Proceedings of ASME Turbo Expo, 2004, GT2004-53842.
[9] L. Magistri, F. Trasino, P. Costamagna, Proceedings of ASME Turbo Expo, 2004, GT2004-53845.
[10] D. Bohn, N. Pöppe, Proceedings of ASME Turbo Expo, 2002, GT-2002-30112.
[11] K. Nishida, T. Takagi, S. Kinoshita, T. Tsuji, Proceedings of ASME Turbo Expo, 2002, GT-2002-30109.
[12] C.W. Hong, N. Watson, SAE International Congress and Exposition, 1988, SAE880122.
[13] N. Watson, M.S. Janota, Turbocharging the Internal Combustion Engine, Macmillan, London/Basingstoke, 1982, pp. 528–529.
[14] U.G. Bossel, Final Report on SOFC Data Facts and Figures, Swiss Federal Office of Energy, Berne, CH, 1992.